JOURNAL OF MATERIALS SCIENCE: MATERIALS IN MEDICINE 15 (2004) 201–208

Stray-field imaging and multinuclear magnetic resonance spectroscopy studies on the setting of a commercial glass-ionomer cement

RICARDO PIRES[1], TERESA G. NUNES[1]*, ISAAC ABRAHAMS[2], GEOFFREY E. HAWKES[2], CLÁUDIA M. MORAIS[3,4], CHRISTIAN FERNANDEZ[4]
[1]*Departamento de Engenharia de Materiais, Instituto Superior Técnico, Universidade Técnica de Lisboa, Av. Rovisco Pais, 1, 1049-001 Lisboa, Portugal*
E-mail: Teresa.Nunes@ist.utl.pt
[2]*Structural Chemistry Group, Department of Chemistry, Queen Mary University of London, Mile End Road, London E1 4NS, UK*
[3]*Departamento de Química, CICECO, Universidade de Aveiro, Campus Universitário de Santiago, 3810-193 Aveiro, Portugal*
[4]*Laboratoire Catalyse et Spectrochimie, CNRS/ENSICAEN, 6 bd du Maréchal Juin, 14050 Caen Cedex, France*

A commercial glass-ionomer (Fuji II) was studied using different NMR techniques. ^{1}H and ^{19}F stray-field imaging (STRAFI) were used to monitor the curing kinetics of the cement and two processes were distinguished: the gelation and maturation phases. Characterization of the aluminium and silicon species present in the glass component and cement was performed by conventional ^{27}Al and ^{29}Si MAS and two-dimensional ^{27}Al triple quantum MAS NMR (MQMAS) techniques. Quantification of the aluminium in the glass component and in the cement indicates the leaching of about 32% of the 4-coordinate aluminium, about 100% of the 5-coordinate aluminium and about 41% of the 6-coordinate aluminium, during the setting reaction. It is also shown that the 5-coordinate aluminium is only present in the surface layer created by the acid attack during the cement formation process. In the cement, silicon maintains species with four bridging oxygens after the leaching of tetrahedral (4-coordinate) aluminium. The silicon analysis correlates well with the aluminium determinations.

1. Introduction

Glass-ionomer cements, described by Wilson and Kent [1] are widely used in restorative dental treatment, and the chemistry of the setting process has been reviewed recently [2, 3]. The glass component is either a calcium or strontium fluoroaluminosilicate material ground to a fine powder and reacted with an aqueous polyalkenoate solution, to form the cement. Fourier transform Infrared spectroscopy has been used [4–6] to demonstrate that the initial reaction (gelation) at the glass particle surface releases calcium ions, which may coordinate and thus crosslink carboxylate groups on the polymer chains. This (i.e. crosslinking by calcium) is followed by formation of aluminium carboxylate crosslinks, which form more slowly and appear to be associated with maturation. The time scales for these two stages are minutes and hours, respectively [3]. Cook [7] showed that aluminium release from the glass occurs in the gelation phase, which confirms that the subsequent reaction of aluminium to form crosslinks is slower than that of calcium. Very long-term changes (weeks/months) in the compressive strength of a cement [8] may be due to the slow splitting of silicate units from the glass structure into the cement matrix [9].

Solid-state ^{27}Al (spin 5/2) and ^{29}Si (spin 1/2) Magic Angle Spinning (MAS) Nuclear Magnetic Resonance (NMR) spectroscopy have been widely used to study aluminosilicates in glass systems [e.g. 10–13]. However, it is only in favourable situations that one-dimensional (1D) ^{27}Al spectral data enable the identification and quantification of species with different aluminium coordination numbers. The 2D ^{27}Al triple-quantum MAS technique (MQMAS) has proved to be a sensitive test for the presence of AlO_5 and AlO_6 species in glasses dominated by AlO_4, such as in magnesium aluminoborate glasses [10]; more recently, the first direct evidence for the presence of a 5-coordinate Al species in $CaAl_2Si_2O_8$ was reported [13]. Under conditions of slow MAS, the ^{27}Al isotropic resonance and its spinning sidebands usually overlap and only qualitative data may

*Author to whom all correspondence should be addressed.

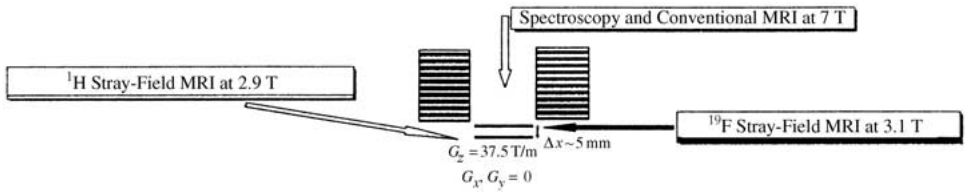

Figure 1 Comparison between NMR spectroscopy and STRAFI MRI on a 7 T magnet.

be extracted from the spectra; this was the case for the ^{27}Al measurements on glass-ionomer cements performed by Matsuya *et al*. [6]. These authors reported that, during the cement formation process, part of the 4-coordinate aluminium changes to a 6-coordinate environment. Matsuya *et al*. [6] also used ^{29}Si MAS NMR to monitor the silicon environment in glass-ionomers and showed that the hydrated silica-gel surface layer recondenses back to a silicon chain after the gelation phase.

Magnetic resonance stray-field (STRAFI) imaging was first introduced by Samoilenko *et al*. [14] and it was used in the study of the curing of Portland cement [15]. The use of STRAFI imaging has also been reported in the case of dental materials. This technique has proved its reliability in the study of the photopolymerization of resin-based dental materials [16, 17] and the proton and fluorine distribution in dental cements [18].

We report here our observations on the setting of glass-ionomer cement using a combination of ^{1}H and ^{19}F STRAFI, ^{27}Al and ^{29}Si MAS and 2D ^{27}Al MQMAS NMR spectroscopy.

2. Materials and methods

The glass-ionomer Fuji II (batch 050391) was obtained from the GC Corporation. The solid component contains a fluoroaluminosilicate glass with calcium replaced by strontium, for greater radiopacity, and polyacrylic acid. The liquid component contains water, polyacrylic acid and tartaric acid. The cement was prepared by mixing the two components (the solid and the liquid), following the instructions of the manufacturers.

STRAFI MRI measurements were performed as previously described [14–16], using a Bruker MSL 300 P NMR spectrometer with an 89 mm diameter bore superconducting solenoid magnet, which generates a magnetic field gradient of 37.5 Tm^{-1} near the edges of the coil. The STRAFI probe was tuned to 123.4 MHz, which gives ^{1}H and ^{19}F resonance at 2.9 and 3.1 T, respectively; these field strengths were obtained just outside the bore of the magnet (see Fig. 1). The spatial separation of the two resonances was 4.9 mm. The samples were contained in cylindrical glass vials, with 4.0 mm length and 6.5 mm inner diameter. The signal of a plastic disc placed outside the vial, in contact with the bottom, was used as a reference. A spacer (a cylindrical piece of ordinary glass not containing hydrogen or fluorine atoms) was introduced between the cement sample and the plastic reference in order to avoid overlap of the ^{19}F sample and ^{1}H reference profiles.

The ^{29}Si MAS NMR spectra were measured at 59.6 MHz, using the Bruker MSL 300 P (7 T) spectrometer, with a spinning speed of 5 kHz. One-dimensional MAS and two-dimensional triple-quantum MQMAS ^{27}Al NMR spectra were recorded at 104.3 MHz, using a Bruker AVANCE 400 (9 T) spectrometer, with a spinning speed of 25 kHz; ^{27}Al 1D spectra at 78.2 MHz were also recorded using the 7 T spectrometer with MAS at 10 kHz. Samples were contained in zirconia rotors with 4 mm or 2.5 mm o.d. for spinning at 5 (or 10 kHz) or 25 kHz, respectively. Isotropic chemical shifts (δ_{iso}) were referenced to external aqueous aluminium nitrate solution (^{27}Al) and to external tetramethylsilane (^{29}Si). Deconvolution of the overlapping resonances was performed using the software programs, MASAI [19] and *dmfit* [20].

3. Results and discussion

3.1. Stray-field imaging

^{1}H and ^{19}F STRAFI profiles of the glass and of the cement cured over 6 weeks are shown in Fig. 2. A very weak ^{1}H signal is detected for the glass, which probably arises from adsorbed moisture and a small amount of polyacrylic acid, together with a clear profile of the ^{19}F magnetization. The strongest signal is observed for ^{1}H in the cement, largely due to the water content. In order to obtain the spatially resolved kinetics for the setting of the cement, profiles were acquired every 10 min during the first 4 h after mixing the cement components, and subsequently, each hour up to a total elapsed time of 65 h. It is observed that the ^{1}H signal intensity decreases with time as shown in Fig. 3(a). The STRAFI MRI

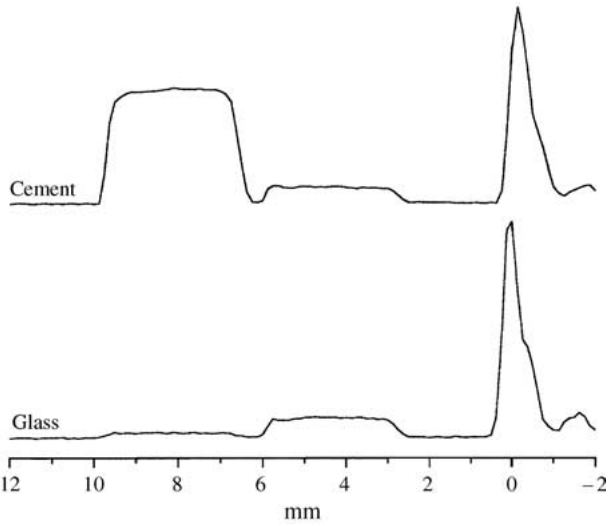

Figure 2 ^{1}H and ^{19}F STRAFI profiles obtained from Fuji II solid component and from the cement cured over 6 weeks. The sharp signal shown on the right side of each profile, also the bottom of the vial, was obtained from a plastic disc used as a reference for intensities (arbitrary units) and for distances (mm).

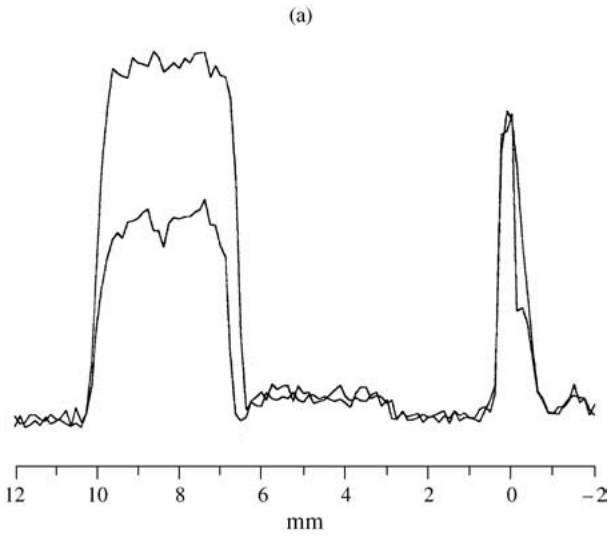

Figure 3 (a) First and final STRAFI profiles obtained during the curing of Fuji II cement over 65 h.

technique allows the observation of both solids (glass and cement) and liquid components (water); the signal intensity depends on hydrogen concentration, but is also strongly affected by relaxation. The relaxation processes are mainly spin–spin and spin–lattice rotating frame relaxation, which are correlated with molecular mobility in the kHz range. They have time constants T_2 and $T_{1\rho}$, which are very short for rigid solids, longer for liquid components. When the total concentration is approximately constant, as during the setting of cement, the decrease of the signal is thus determined by the gel–solid phase transition. As the setting progresses and the material becomes more rigid, it is then expected that the average ^{1}H T_2 decreases, thereby decreasing the intensity of the profile [15]. The time dependence of the intensity at three different positions through the profile (Fig. 3(b)) was fitted with a double exponential function. The t_1 and t_2 time constants resulting from these fits are given in Table I. The average short- and long-time constants, 29 min and 25 h, respectively, would appear to correlate well with the initial gelation phase, followed by the maturation phase. We are unable to fully explain the variation in time constants with position, however, it must be pointed out that sedimentation and water evaporation are expected to contribute to the spatial variation of the kinetics, especially during the early reaction period.

TABLE I Time constants of the double exponential functions that best fit the indicated slice intensity decay of the ^{1}H STRAFI MRI profiles acquired over 65 h

Slice, d (mm)	t_1 (min) (%)	t_2 (h) (%)
Top, 9.8	25 ± 1	28 ± 2
Middle, 8.5	36 ± 2	27 ± 1
Bottom, 7.1	25 ± 1	19 ± 1

d is the distance of the slice to the plastic disc used as a reference (see Fig. 2).

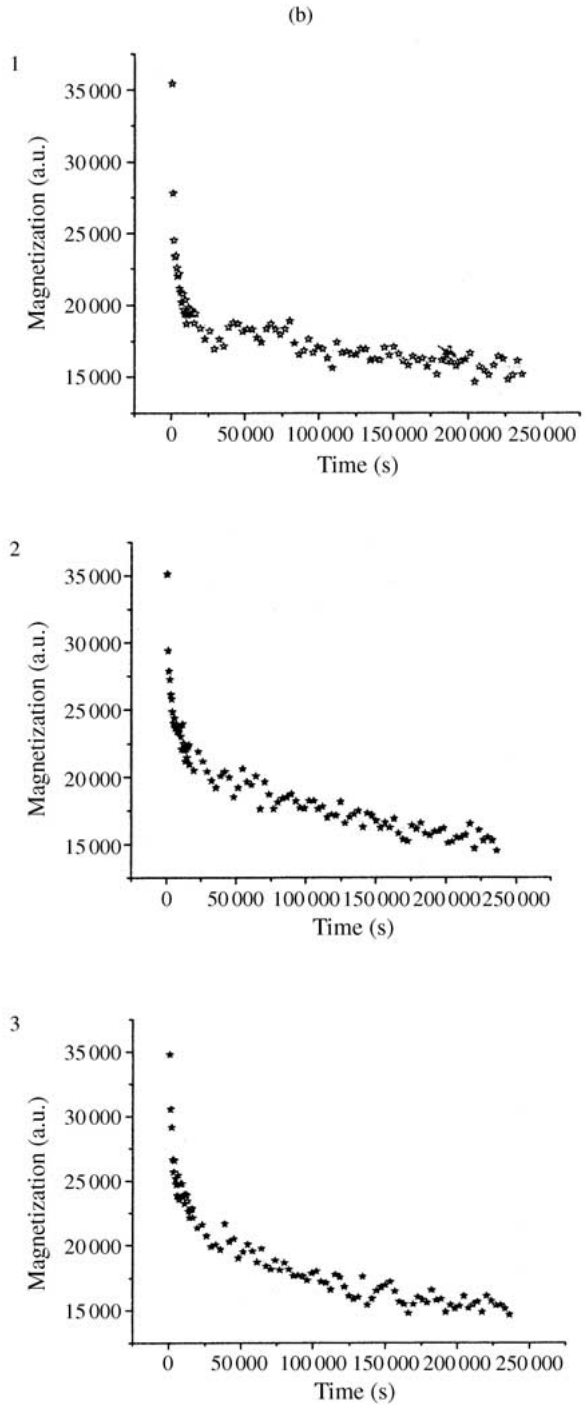

Figure 3 (b) Double exponential decay fittings of the magnetization intensity variation on three different slices in the cement at the indicated distances from the plastic disc used as a reference (see Fig. 2): (1) top slice at 9.8 mm; (2) middle slice at 8.5 mm; (3) bottom slice at 7.1 mm.

3.2. ^{27}Al MAS NMR spectra

The central transition (CT) frequency of the spectrum of a quadrupolar nucleus of half integer spin, such as ^{27}Al ($I = 5/2$), depends on the orientation of each crystallite in the static magnetic field, to second order in perturbation theory. The quadrupolar interaction between the nuclear electric quadrupole moment (eQ) and the electric field gradient at the nucleus (eq), arising from any lack of symmetry in the local electron distribution, is described by the quadrupolar coupling constant $C_q(e^2qQ/h)$ and the asymmetry parameter η. It must be noticed that disordered materials, such as glasses and cements, have a

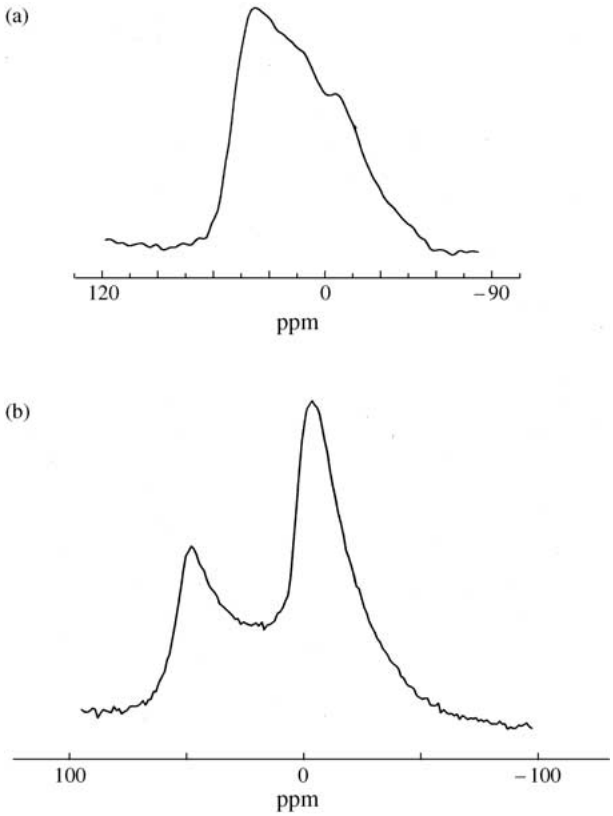

Figure 4 (a) 78.2 MHz ^{27}Al MAS NMR spectrum of the solid glass component. (b) 78.2 MHz ^{27}Al MAS NMR spectrum of the cement.

wide range of interatomic distances and, consequently, CT line broadening occurs due to the distribution of δ_{iso} and quadrupolar interactions. One-dimensional ^{27}Al MAS (7 T) NMR spectra of the glass and the cement (cured over 17 months) are shown in Fig. 4(a) and (b), respectively. Fig. 4 shows a number of overlapping resonances and a correct deconvolution of the CT lines requires a prior knowledge of δ_{iso} and C_q distribution for each of the lines. By recording 2D MQMAS (9 T) spectra, from the glass and from the cement, we are able to obtain the number of different aluminium species and an estimation of the corresponding δ_{iso}, quadrupolar parameters and distribution. The results are in agreement with at least three different aluminium sites in the glass (Fig. 5(a1)) and four in the cement (Fig. 5(a2)). To obtain the NMR parameters of each aluminium species, we have used MASAI, a homemade simulation program [19], which assumes a Gaussian distribution of δ_{iso} and of the principal components of the electric field gradient tensor, in order to simulate 1D and 2D spectra run at 9 T. The Tables II and III show the results obtained using the program MASAI for the glass and for the cement, respectively; Fig. 5(b) shows the 1D MAS spectra and the simulated lines. It is well known that the isotropic chemical shifts depend on the aluminium coordination number; in crystalline aluminosilicate materials, 6-coordinate aluminium like AlO_6, has δ_{iso} about 1–15 ppm (C_q between 1 and 10 MHz), 4-coordinate aluminium AlO_4, has δ_{iso} in the range 55–88 ppm (typically C_q also between 1 and 10 MHz) and δ_{iso} is about 30–40 ppm for 5-coordinate species AlO_5 (C_q between 3 and 10 MHz) [10]. On this basis, the changes in aluminium environment are clearly observed by

TABLE II Concentration and NMR parameters for the ^{27}Al species in the Fuji II glass, obtained by fitting the experimental 1D spectra recorded at 9 T using the software program MASAI[a] [19]

Species	Concentration (%)	δ_{iso} (ppm)	C_q (MHz)
1	74	59 ± 6	6.5 ± 2.3
2	15	28.3 ± 6.8	5.6 ± 2.0
3	11	-0.5 ± 4.1	4.8 ± 2.7

[a]This program also uses MQMAS spectra for the fitting.

TABLE III Concentration and NMR parameters for the ^{27}Al species in the Fuji II cement, obtained by fitting the experimental 1D spectra recorded at 9 T using the software program MASAI[a] [19]

Species	Concentration (%)	δ_{iso} (ppm)	C_q (MHz)
1	45.5	60.0 ± 5.8	6.5 ± 2.3
2	4.5	57.3 ± 2.0	3 ± 1
3	45.5	5.3 ± 2.9	4.0 ± 2.8
4	4.5	-2.0 ± 4.5	3 ± 1

[a]This program also uses MQMAS spectra for the fitting.

comparing the MQMAS spectra of both the glass and the cement. The NMR data given in Tables II and III are consistent with the presence of 74% of aluminium in the tetrahedral environment (4-coordinate) in the glass, which is reduced to an overall of about 50% in the cement. It is also noted that instead of only one highly distributed 4-coordinate species initially present in the glass ($\delta_{iso} \approx 59$ ppm, Fig. 5(a1)), two distinct sites are present in the cement particles ($\delta_{iso} \approx 60$ and 57 ppm, Fig. 5(a2)). There is 15% of the 5-coordinate aluminium species in the glass that is not detected in the cement. Assuming that all aluminium is detected, the decreases observed for both 4- and 5-coordinate aluminium species is compensated by an increase in the amount of 6-coordinate aluminium species that changes from an overall 11–50%. We note that two 6-coordinated Al sites are present in the final cement (Figs. 5(a2) and (b2)), instead of only one as in the precursor glass (Figs. 5(a1) and (b1)). 4-Coordinate aluminium, with effectively tetrahedral coordination geometry is likely to act as network former in the aluminosilicate glass, whereas 5- and 6-coordinate aluminium species are likely to act as network modifiers.

Our interpretation of these NMR data considers the glass particles (G) to comprise a reactive surface layer (SL) and an inert core (CO). Cement formation occurs by reaction between the liquid component of Fuji II (the aqueous polyacid) and the glass particles' surface layer. The cement matrix is defined here as the interstitial material linking the residual glass particles.

The glass particle surface layer is created during the setting of the cement, which is initially a gel. In this layer it is expected that 5- ($\delta_{iso} \approx 28$ ppm) and 6-coordinate ($\delta_{iso} \approx 0$ ppm) aluminium species are leached out into the cement matrix (CM), but the 4-coordinate aluminium species, which is more covalently bound and less susceptible to the acid attack is leached out to a lesser extent. It is thus expected that a certain amount of this 4-coordinate aluminium in the SL will not be leached to the CM.

As working hypothesis, we propose that the 4- and

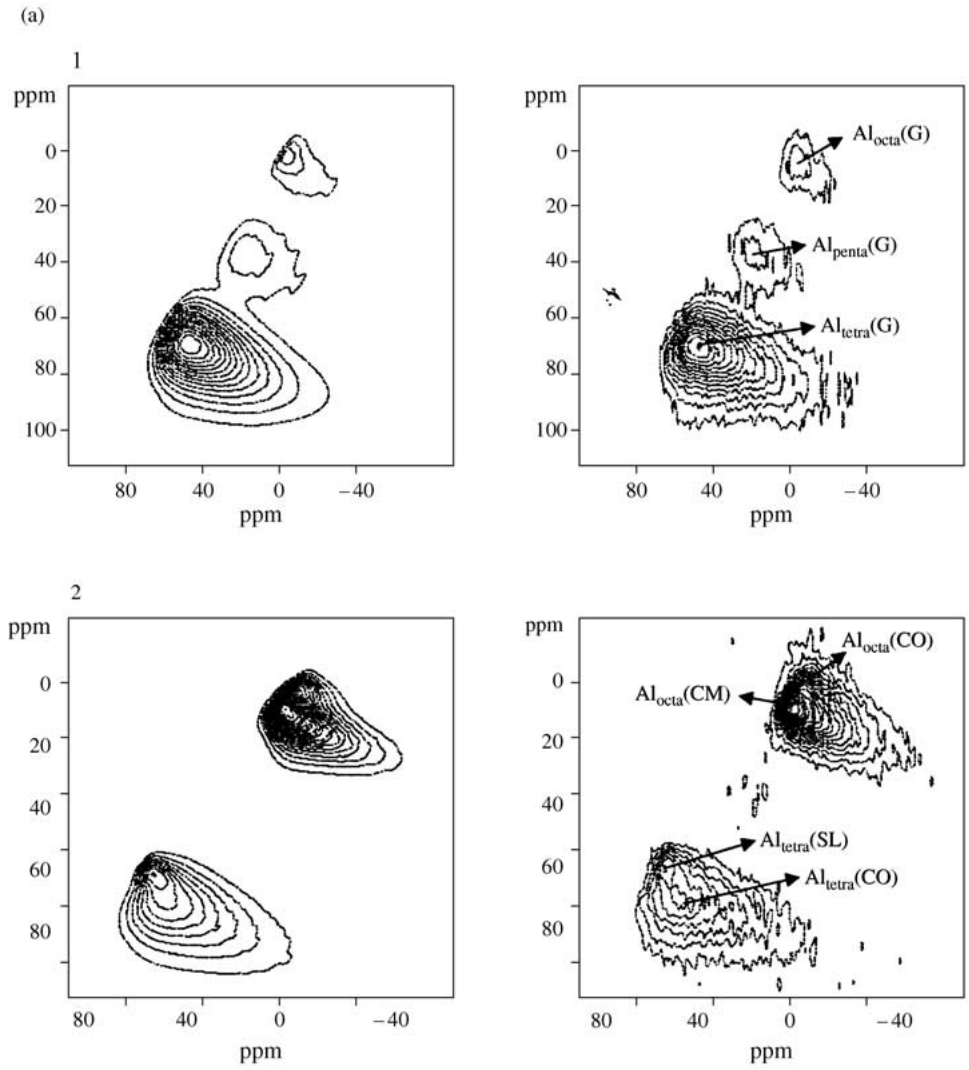

Figure 5 (a) 104.3 MHz ^{27}Al MQMAS NMR spectrum of the solid glass component and of the cement, showing the assignment of the different aluminium species: (1) Experimental (right side) and simulated spectra of the glass; (2) Experimental (right side) and simulated spectra of the cement. The simulated spectra were obtained with the software program MASAI [19].

6-coordinate aluminium species are distributed homogeneously between the surface and the core of the glass particle. However, the complete absence of the 5-coordinate aluminium signal from the cement sample indicates this species to be present only in the reactive SL of the glass particles. Octahedral (6-coordinate) aluminium in the CM (Al_{oct}(CM)) is derived from three sources: all the 5-coordinate aluminium in the SL of the glass (Al_{penta}(SL)); a proportion (x) of the 4-coordinate aluminium in the original unreacted glass ($Al_{tetra}(G)$); a proportion (y) of the 6-coordinate aluminium in the original unreacted glass ($Al_{octa}(G)$).

$$Al_{octa}(CM) = Al_{penta}(SL) + xAl_{tetra}(G) + yAl_{octa}(G) \quad (1)$$

The total 4-coordinate aluminium in the whole cement amounts to ca. 50%, which is the sum of the two environments (45.5 and 4.5% for species 1 and 2 in Table III). The more abundant of these two environments has the much larger quadrupolar coupling (C_q ca. 6.5 MHz) and is assigned to 4-coordinate aluminium in the unreacted core of the glass particle. Correspondingly the lower abundant environment (species 2 in Table III) is assigned to residual 4-coordinate aluminium in the glass particle SL after cement formation.

The 45.5% core 4-coordinate aluminium in the whole cement corresponds to the content of the unreacted glass. Therefore, 28.5% of the 4-coordinate aluminium in the initial glass originates in the SL and 24% is leached out during the cementation reaction (see Scheme 1). On this basis a proportion 28.5/74 of the 4-coordinate aluminium resides in the SL of the precursor glass particles. With the premise of the homogeneous distribution of the 4- and 6-coordinate aluminium, the 11% 6-coordinate aluminium in the unreacted glass should be distributed as approximately 6.8% core and 4.2% SL. Figs. 5(a2) and (b2) indicates the presence of two 6-coordinate ^{27}Al signals, and to be consistent with the above argument, the less intense signal (species 4, 4.5%, see Table III) is from the surface layer of the glass particles while species 3, more abundant, is from the CM (45.5%). To summarize, the 11% 6-coordinate aluminium in the unreacted glass is distributed as approximately 6.5% core and 4.5% SL

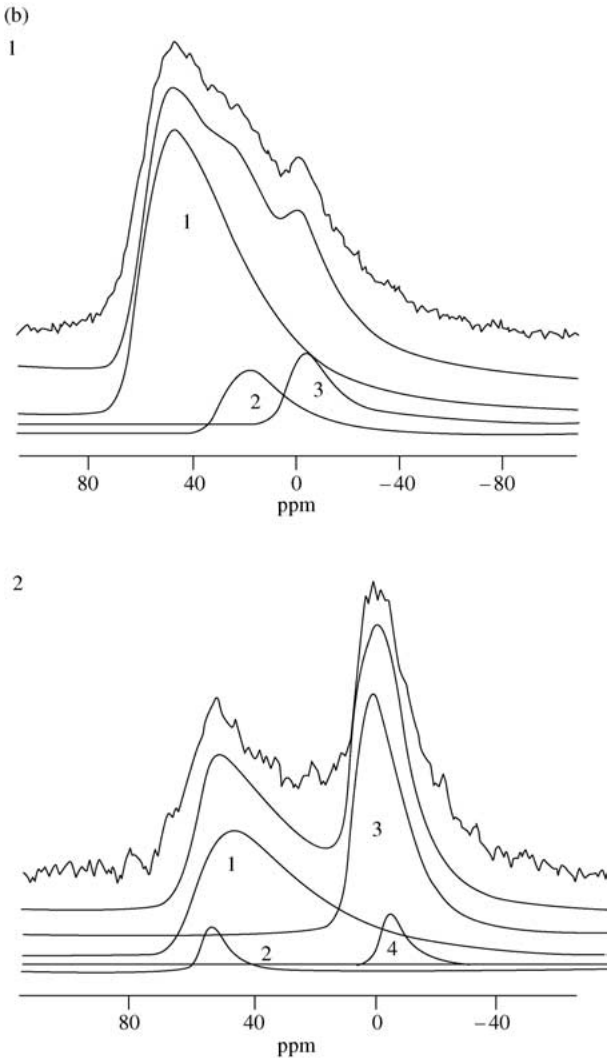

Figure 5 (b) Experimental and simulated 104.3 MHz ^{27}Al MAS NMR spectra of: (1) the solid glass component, showing the lines 1–3 that correspond to the three aluminium sites; (2) the cement, showing the lines 1–4 that correspond to the four aluminium sites. The simulated spectra were obtained with the software program MASAI [19].

(species 3 and 4 in Table III). With these data the values (Equation 1) are derived $x = 0.32$ and $y = 0.41$; i.e. about 32% of the 4-coordinate and 41% of the 6-coordinate aluminium species are leached out of the glass upon reaction.

The reactions of the various aluminium species are summarized in Scheme 1.

3.3. ^{29}Si MAS NMR spectra

The ^{29}Si MAS NMR spectra of the glass and the cement clearly comprise overlapping resonances, and deconvolution gave the major component resonances in Tables IV and V. Figs. 6(a) and (b) show the deconvolution of the spectra performed with the *dmfit* software program [20] for the glass and cement, respectively. In the fitting procedure a Gaussian lineshape was assigned to all the major ^{29}Si resonances. The resonances are assigned using the Q^n nomenclature, where n is the number of bridging oxygens bound to silicon, and the number of nearest neighbour aluminium atoms is given in parentheses. Thus Q^4(3 Al) is:

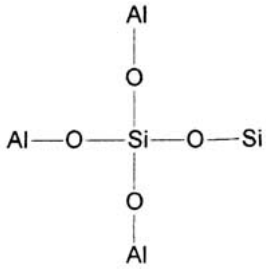

Because the reported [21] chemical shift ranges overlap, the resonances at -93 and -94 ppm for the glass can be due to either Q^4(2 Al) or Q^4(3 Al). The resonances at -87 ppm are assigned in Tables IV and V to Q^4(4 Al) or Q^4(3 Al), but we consider the additional possibility that this chemical shift may also arise from Q^3(3 Al):

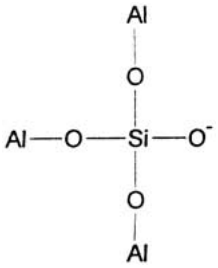

Glass (before reaction)	
Coordination	Mol %
4	74
4	0
5	15
6	0
6	11

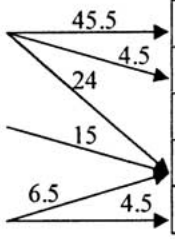

Whole cement	
Mol %	Coordination
45.5	4
4.5	4
0	5
45.5	6
4.5	6

TABLE IV Components of ^{29}Si resonances in Fuji II glass obtained by signal deconvolution using the software program *dmfit* [20]

Signal	δ (ppm)	Concentration (%)	Species[a]
1	−87	7	Q^4(3/4 Al)[b]
2	−93	16	Q^4(2/3 Al)[c]
3	−94	77	Q^4(2/3 Al)[c]

[a]Assignments made by comparison with the data of [21].
[b]The chemical shifts could arise from Q^4 silicon with either 3 or 4 nearest neighbour 4-coordinate aluminium atoms.
[c]The chemical shifts could arise from Q^4 silicon with either 2 or 3 nearest neighbour 4-coordinate aluminium atoms.

TABLE V Major components[a] of ^{29}Si resonances in Fuji II cement obtained by signal deconvolution using the software program *dmfit* [20]

Signal	δ (ppm)	Concentration (%)	Species[b]
1	−87	16	Q^4(3/4 Al)[c]
2	−92	25	Q^4(3 Al)
3	−99	33	Q^4(1/2 Al)[d]
4	−109	24	Q^4(0 Al)

[a]Minor resonances with integral $< 2\%$ not included.
[b]Assignments made by comparison with the data of [21].
[c]The chemical shifts could arise from Q^4 silicon with either 3 or 4 nearest neighbour 4-coordinate aluminium atoms.
[d]The chemical shifts could arise from Q^4 silicon with either 1 or 2 nearest neighbour 4-coordinate aluminium atoms.

Moreover, for the cement, the signal observed at −92 ppm could be assigned to Q^3(0 Al). In spite of the uncertainty in assignment, it is clear from the data in Tables IV and V that cement formation results in an overall decrease in the number of nearest neighbour aluminium atoms.

In order to obtain an estimate for the quantitative ratio of tetrahedral Si to Al in the network structure, we have calculated the limits by using the formula $\mathrm{Si/Al} = (\sum I_{4,m} / \sum (m/4) I_{4,m})$ where $I_{4,m}$ are the intensities of $Q^4(m\mathrm{Al})$ units and the summation run from $m = 0$ to 4. By assigning to each species the unit with the highest or the lowest number of Al atoms, the lowest and the highest Si/Al ratio were obtained: 1.3–1.9 for the glass and 1.9–2.5 for the cement. Applying the results obtained by ^{27}Al MAS NMR (68% of the tetrahedral aluminium does not change its coordination) to the calculated tetrahedral Si/Al ratio in the glass, it is expected that the Si/Al ratio in the cement should be 1.9–2.8, which is in agreement with the range obtained by ^{29}Si MAS NMR. This result is entirely consistent with the conversion of part of the 4-coordinate (covalent) aluminium in the glass network to 6-coordinate (ionic) aluminium upon cement formation, as shown by the ^{27}Al spectra. In the glass network structure each aluminium bridges nearest neighbour silicon tetrahedra. Therefore, when this aluminium is removed from the network structure, the silicon tetrahedra must condense in order to preserve the Q^4 content:

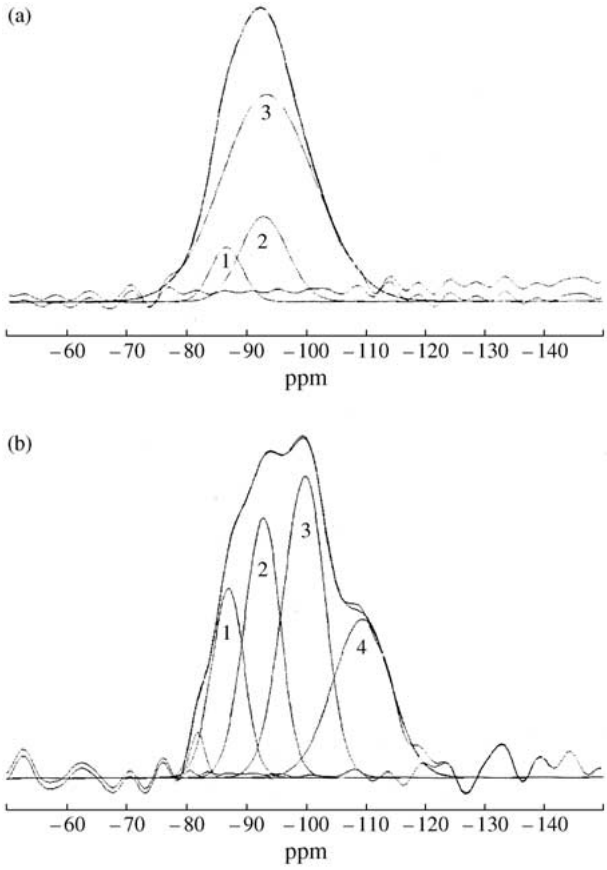

Figure 6 (a) Fitting of the ^{29}Si MAS NMR of the Fuji II glass component, using the program *dmfit* [20]. (b) Fitting of the ^{29}Si MAS NMR of the Fuji II cement, using the program *dmfit* [20].

The leaching of aluminium ions from the glass network that we detect is only from the 4-coordinated species that are present as glass formers and in the SL. It is important to point out that the silicon species present in the glass should also be present in the cement in the glass particle core. The Q^4(4 Al) silicon is more susceptible to the acid attack because of the higher concentration of aluminium atoms.

4. Conclusions

These magnetic resonance experiments are complementary and are consistent with recent proposals on cement formation [2, 3]. The analysis of the STRAFI data shows two processes occurring, one corresponding to the initial gelation phase (time constant 25–36 min), and the other to the slower maturation phase (time constant 19–28 h). In the gelation phase available ions are leached out from the glass, and these cations are Al^{3+} initially present in the glass in a 5- and 6-coordinate environment and Sr^{2+}. During the maturation phase part of the covalent bound tetrahedral aluminium (network forming) is leached out. This process is slower because the more covalent aluminium–oxygen bonds must be broken, and in the

process 4-coordinate aluminium is converted to 6-coordinate aluminium. All 5- and 6-coordinate aluminium present in the range of the glass particle SL, created by the acid attack, is leached out of the glass. Additionally, the non-detection of the 5-coordinate aluminium in the cement indicates that this species is only present in the SL. Overall, about 32% of the 4-coordinate, 100% of the 5-coordinate and 41% of the 6-coordinate aluminium species are leached out of the glass during the cement formation process. From the ^{29}Si MAS NMR spectra of the glass, the tetrahedral Si/Al ratio should be 1.3–1.9 and, considering that, from the ^{27}Al MAS NMR, 68% of the tetrahedral aluminium should maintain its coordination, it is expected that the Si/Al ratio changes to 1.9–2.8, which is in good agreement with the values obtained by the analysis of the ^{29}Si MAS NMR spectra of the cement, 1.9–2.5. Moreover, to preserve the observed Q^4 speciation at silicon, following leaching out of network forming aluminium, the silica tetrahedra must condense back to Q^4.

The present study is now being extended to a hybrid ionomer (FUJI II LC) in order to evaluate the influence in the cement composition and setting kinetics of the liquid component, which contains monomers that undergo a light-cure reaction.

Acknowledgments

This study was supported by the Portuguese Foundation for Science and Technology-EEC research program (Project: POCTI/33193/FCB/2000). R.P. acknowledges a PRAXIS XXI PhD research grant (BD/21572/99). Thanks are due to Prof. João Rocha for the facilities to perform the MAS and the MQMAS experiments at 9 T.

References

1. B. E. KENT and A. D. WILSON, *Br. Dent. J.* **135** (1973) 322.
2. J. W. NICHOLSON, *Biomaterials* **19** (1998) 485.
3. B. M. CULBERTSON, *Progr. Polymer Sci.* **26** (2001) 577.
4. S. CRISP, M. A. PRINGUER, D. WARDLEWORTH and A. D. WILSON, *J. Dent. Res.* **53** (1974) 1414.
5. J. W. NICHOLSON, P. J. BROOKMAN, O. M. LACY and A. D. WILSON, *ibid.* **67** (1988) 1451.
6. S. MATSUYA, S. MAEDA and M. OHTA, *ibid.* **75** (1996) 1920.
7. W. D. COOK, *J. Biomed. Mater. Res.* **17** (1983) 1015.
8. E. A. WASSON and J. W. NICHOLSON, *J. Dent. Res.* **72** (1993) 481.
9. A. D. WILSON, *J. Mater. Sci. Lett.* **15** (1996) 275.
10. J. H. BALTISBERGER, Z. XU, J. F. STEBBINS, S. H. WANG and A. PINES, *J. Am. Chem. Soc.* **118** (1996) 7209.
11. M. SCHMUCKER, M. SCHNEIDER, K. J. D. MACKENZIE and M. OKUNO, *J. Eur. Ceram. Soc.* **19**(1) (1999) 99.
12. F. ANGELI, J.-M. DELAYE, T. CHARPENTIER, J.-C. PETIT, D. GHALEB and P. FAUCON, *Chem. Phys. Lett.* **320** (2000) 681.
13. J. F. STEBBINS, S. KROEKER, S. K. LEE and T. J. KICZENSKI, *J. Non-Cryst. Solids* **275** (2000) 1.
14. A. A. SAMOILENKO, D. Y. ARTEMOV and A. L. SIBEL DINA, *JETP Lett.* **47** (1988) 348.
15. T. NUNES, E. W. RANDALL, A. A. SAMOILENKO, P. BODART and G. FEIO, *J. Phys. D: Appl. Phys.* **29** (1996) 805.
16. T. G. NUNES, R. PIRES, J. PERDIGÃO, A. AMORIM and M. POLIDO, *Polymer* **42** (2001) 8051.
17. T. G. NUNES, G. GUILLOT, S. G. PEREIRA and R. PIRES, *J. Phys. D: Appl. Phys.* **35** (2002) 1251.
18. C. H. LLOYD, S. N. SCRIMGEOUR, G. HUNTER, J. A. CHUDEK, D. M. LANE and P. J. MCDONALD, *J. Mater. Sci: Mater. Med.* **10** (1999) 369.
19. C. FERNANDEZ, A. A. QUOINEAUD, V. MONTOUILLOUT, S. GAUTIER and S. LACOMBE, *Stud. Surf. Sci. Catal.* **135** (2001) 183.
20. D. MASSIOT, F. FAYON, M. CAPRON, I. KING, S. LE CALVÉ, B. ALONSO, J. O. DURAND, B. BUJOLI, Z. GAN and G. HOATSON, *Magn. Reson. Chem.* **40** (2002) 70.
21. G. ENGELHARDT and H. KOLLER, in ''Solid-State NMR II: Inorganic Matter'', edited by P. Diehl, E. Fluck, H. Gunther, R. Kosfelf and J. Seelig (Springer-Verlag, 1994) p. 15.

Received 30 April
and accepted 18 September 2003